3D PRINTING FOR PROTOTYPES OF THIN-FILM PZT/POLYMER MICROSTRUCTURES

Clark B. Teeple, Jinhong Qu, Kenn R. Oldham
Dept. of Mechanical Engineering, University of Michigan, Ann Arbor, MI

Abstract

This work explores the viability of using 3D printing as a rapid-prototyping technique for micro-robotic appendages made from thin-film PZT/polymer materials. First, the possibility of integrating piezoelectric materials into millimeter-scale (meso-scale) polymer melt-printed structures was investigated. Next, one specific robot limb geometry was chosen as a basis to compare structural modeling techniques and perform scaling analysis. Scaling was performed to select the dimensions of one micro-scale device and two differently-sized prototypes. Beam-bending analysis was used to produce a simple analytical model, and finite element analysis was used to generate more accurate computational models. One size of devices has been fabricated to date, and its dynamic behavior was tested. From modeling and experiments, integrating PZT into the printing process was determined to be non-trivial. Additionally, the two modeling techniques predict static behavior relatively close to each other. However, the fabricated Large Printed limb exhibited static behavior much smaller than the models predict. Finally, the scaling analysis produces predictable results for the small printed device, but shows poor accuracy for the large printed device. Based on these results, we conclude that, while more investigation is necessary, 3D printing shows promise for prototyping of thin-film PZT/polymer microrobots.

Introduction

A wide range of micro robots are currently being explored for a variety of applications. For example, a sub-millimeter swimming micro robot utilizing a piezoelectric micro-motor has been proposed for navigation inside blood vessels in the human body [1]. In another set of studies, flying microrobots have been extensively designed and studied for surveillance and search-and-rescue applications [2]. Further, much work has been completed investigating micro-scale walking robots. One walking robot was designed to be controlled with a neural network [3].

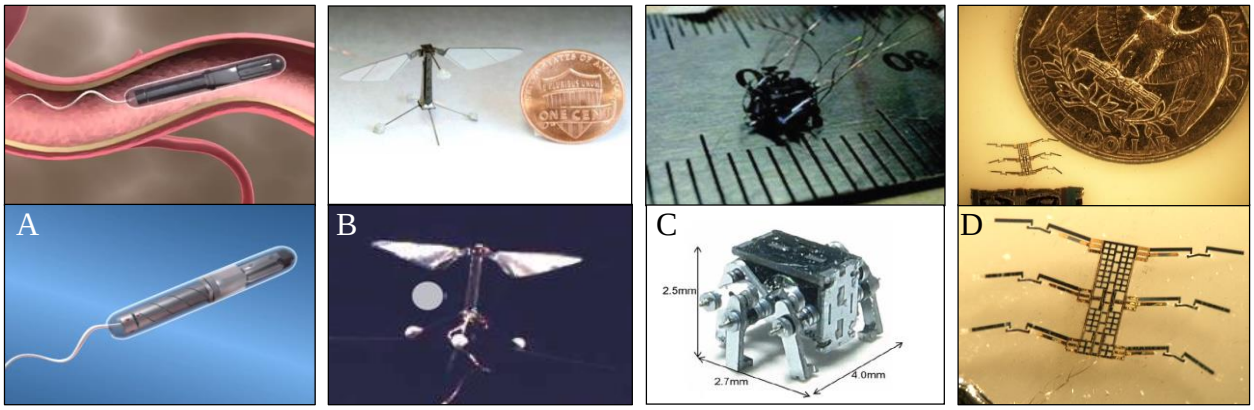

Figure 1. Several microrobots currently being explored for a variety of applications. (A) swimming robot for navigation inside the human body [1], (B) flying robot for surveillance [2], (C) walking robot controlled by a neural network [3], and (D) hexapod robot with thin-film piezoelectric actuators and integrated polymer for search-and-rescue [4].

Another insect-inspired hexapod robot was demonstrated to exploit thin-film piezoelectric actuators and flexible polymer structures with applications in search-and-rescue [4]. These robots can be seen in Fig. 1.

Thin-film piezoelectric microrobots, like the one shown in Fig. 1D, use a thin layer of lead-zirconate-titanate (PZT) along with electrode layers on a silicon substrate. In addition, high-aspect ratio parylene polymer beams are used as flexural mechanisms to form a leg structure. This construction allows for large in-plane stiffness, but small out-of-plane stiffness, which can improve load-carrying capacity of the robot [5].

While all of these microrobots show promise, a few basic challenges emerge with regard to fabrication of these devices. Processing techniques can be expensive and involve long wait times. In addition, the materials used can be fragile at the micro-scale dimensions these robots use, which results in very fragile robotic structures. Thus, fragile microrobots can be difficult to assemble, and have a high failure rate. For example, as shown in Fig. 2, a legged microrobot was fabricated with a silicon body, and piezoelectric actuators were added later [6]. The process of attaching the actuators to the body was tedious, and in this case two of the feet were already broken to begin with. Even after many complicated and expensive fabrication steps, microrobots tend to be fragile and have a very high rate of fabrication failure and variability.

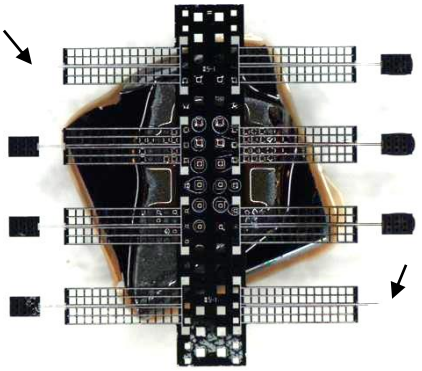

Figure 2. Microrobot designed for later addition of piezoelectric actuators [6]. Arrows show locations of missing feet

One way to circumvent (or at least investigate) these fabrication challenges is to use physical prototypes. Prototypes are used throughout engineering as a means of quickly testing the feasibility of new designs. For microrobots, prototyping generally involves scaling up the dimensions of the microrobot into the millimeter or centimeter (meso) scale. This is a way to attain quick proof of concept for new actuation mechanisms or body designs. In addition, prototypes can be used to test behaviors that are not well-captured by modeling, especially robots with complex geometries that would otherwise be impossible to model. Physical prototypes can also provide a test-bed for power electronics. Finally, prototypes can offer a convenient way to study contact dynamics and ground interactions because micro-scale robots are often difficult to characterize and measure accurately. In addition, contact dynamics are hard to simulate, especially for microrobots with multiple legs. At the micro-scale, all parts of the body are flexible, and vibrations occur across the entire body, which poses challenges for even finite element modeling. Thus, meso-scale prototypes have been used in place of micro-scale robots to extensively study contact dynamics of small walking robots [7].

Several rapid-prototyping technologies exist for small-scale devices. For example, photolithography is an effective way to generate micro-channels for microfluidic devices, and can be done quickly and at low cost with the aid of a high-resolution inkjet printer [8]. Additionally, micro-stereolithography has been used to generate complex 3D structures with micron-scale features [9]. In a different approach, prototypes of millimeter-scale robots were generated on a larger scale using cheap cardboard-type material and cheaper actuation methods

than the smaller scale device [10]. Finally, 3D printing using a melted polymer filament is quickly becoming the rapid-prototyping technique of choice for meso and macro-scale objects.

For our PZT and polymer integrated microrobots, a rapid-prototyping method using meso-scale prototypes generated quickly and cheaply could streamline the design process and offer new opportunities to study behavior. Thus, 3D printing presents the best solution. However, little work has been done to investigate how behavior of meso-scale prototypes can be used to understand behavior of the actual micro-scale robots. This study was set forth to evaluate 3D printing as a rapid prototyping technique for prototypes of PZT and polymer integrated microrobots. Specifically, interest exists in finding ways to integrate meso-scale piezoelectric actuators into the printing process. From there, we are interested in assessing the static and dynamic behaviors of printed prototypes as compared with analytical and finite elements models. Finally, we are interested in how these behaviors scale down to the micro-scale robots. The purpose of this paper is to report our findings in this investigation thus-far.

Methods

In order to evaluate the viability of 3D printing for generating prototypes of thin-film microrobots, first the capabilities of a high-resolution consumer 3D printer were evaluated. Then a simple robot limb design was chosen that would be easy to model and fabricate. Dimensional analysis was used to determine how static behavior of the limb scales with size and materials. Based on this analysis and printing capabilities, two sizes of printed prototypes were determined, along with a theoretical microscale device. The behavior of this limb design was modeled using analytical beam bending analysis as well as finite element analysis (FEA). Finally, the large printed limb was fabricated, and its dynamic behavior was experimentally determined, allowing its static behavior to be inferred.

3D printing capabilities: In order to fabricate 3D printed prototypes of thin-film microrobots, an Ultimaker 3D printer (Ultimaker Original [11]) was chosen because of its extremely high vertical resolution (nominally 20 μm). High vertical resolution is desirable to replicate thin-film devices. This printer uses heated nozzle to deposit PLA polymer layer-by-layer. After experimenting with various parameters in both software and hardware, it was determined that a structure with less than four layers is not feasible to print due problems removing the finished part from the stage after printing. Additionally, the smallest reliable height step was found to be 60 μm, yielding a minimum printable height of approx. 0.240 mm. Furthermore, the lateral resolution of the printer is much lower due to the drive mechanisms and nozzle diameter (0.4mm). The minimum lateral resolution for a printed structure was found at be approx. 0.5 mm.

To evaluate the possibility of integrating piezoelectric actuators into the printing process, standard off-the-shelf PZT strips (31.8 mm × 3.2 mm, thickness 0.48 mm), were tested using printed structures specifically designed to incorporate them. The printed polymer had trouble adhering to the smooth surface of the PZT. Also, the strip's shape and size were hard to control precisely enough to facilitate printing. Additionally, while not a concern for this actuator, other piezoelectric materials are temperature sensitive, so the hot nozzle would pose problems for integration of these strips into the printing process. Thus, at this time, attaching piezoelectric actuators to the printed polymer body can only feasibly be done using adhesives such as epoxy.

Design of a simple microrobotic limb: For this study, it was necessary to develop a simple robot design that is easy to model and fabricate. Inspired by mechanisms used in more complex thin-film microrobots, a simple microrobotic limb was conceived, as shown in Fig. 3. The limb has a polymer body with two independent PZT bending actuators attached at each leg. The actuators can be operated in-phase (same direction), or out-of-phase (opposite directions) with respect to time. The in-phase mode provides pure bending in the legs, causing the foot to travel vertically without rotation in the x-axis. The out-of-phase mode produces torsion, causing the foot to rotate about the x-axis, with minimal vertical displacement. Thus, the single, simple design is capable of achieving both simple and relatively complex motion.

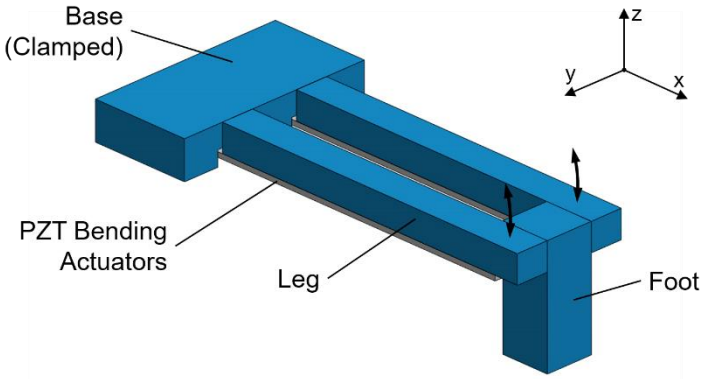

Figure 3. Simple microrobotic limb design chosen for this study has a polymer body (blue) and two independent PZT bending actuators (gray). The actuators can create pure bending in the legs when operating in-phase, and torsion of the foot when operating out-of-phase. The base enforces a ground boundary condition at the base of the legs.

Scaling and dimensions of different-sized limb structures : Now that a test structure geometry (the limb design) was established, the next step was to determine how its behavior scales with different lengths and materials in order to set the actual dimensions of micro-scale and meso-scale limbs. Using dimensional analysis, the static behavior of the limb as a function of non-dimensional groups was established. The goal was then to keep as many of these groups constant as possible. However, the properties and dimensions of the piezoelectric strips at both the micro and meso-scale were fixed based on availability and processing techniques, so several terms such as ratio of elastic moduli and thickness of the piezoelectric strip could not be held constant across length scales. Consequently, not all groups that would ideally be fixed were held constant when scaling. To partially compensate for this, a vertical stiffness group was introduced instead, encompassing both un-scalable groups. The resulting non-dimensional groups held constant are shown in Eq. 1-3,

$$\Pi_1 = \frac{t_{poly}}{L}, \quad \Pi_2 = \frac{t_{foot}}{L}, \quad \Pi_3 = \frac{t_{piezo}^3 E_{piezo}}{t_{poly}^3 E_{poly}} \qquad \text{(Eq. 1-3)}$$

where Π represents a non-dimensional group, *t* refers to the thickness in the z-direction, *L* is characteristic length (set as the length of the leg in the x-direction), *E* is Young's modulus, subscript "*poly*" refers to the polymer portion of the leg (Parylene or PLA) , "*piezo*" refers to the PZT actuator portion, and "*foot*" refers to the foot.

Next, three non-dimensional groups were considered as variables, shown in Eq. 4-6,

$$\Pi_4 = \frac{V d_{31}}{t_{piezo}}, \quad \Pi_5 = \frac{R_y}{L^2 E_{poly}}, \quad \Pi_6 = \frac{R_z}{L^2 E_{poly}} \qquad \text{(Eq. 4-6)}$$

where *V* is voltage applied to the PZT actuators, d_{31} is the piezoelectric constant of the actuators, R_y and R_z are the reaction forces in the y and z-directions at the base of the foot. Since the y and z

reaction forces were assumed to be de-coupled, dimensionless foot displacements Δy and Δz (pertinent outputs) were produced as a function of only two variables, as shown in Eq. 7 and 8.

$$\frac{\Delta y}{L} = f(\Pi_4,\ \Pi_5), \qquad \frac{\Delta z}{L} = f(\Pi_4,\ \Pi_6) \qquad \text{(Eq. 7, 8)}$$

Using Π_1 and Π_3, the minimum printing capabilities of the 3D printer, and the sizes of available PZT actuators, dimensions for three sizes of limbs were found, as shown in Fig. 4. The Micro limb is based on the thickness of polymer and PZT that are commonly used in fabrication of microrobots and will be subjected to small-scale forces such as electrostatics and squeeze-film damping. The Small Printed limb was chosen at the lower limits of printer capability, uses a single-layer PZT strip, and is approaching the size where small-scale forces start to appear, however it will be difficult to fabricate. The Large Printed limb is based on standard double-layered PZT strips, creating a ~3cm device that is easy to fabricate and assemble, but does not capture small-scale force effects. The material properties and pertinent dimensions of the limb structures are shown in Table 1.

Table 1: Material properties and important dimensions of the three simple limb devices, along with length scale compared to the Micro device.

Parameter	Unit	Micro	Small Printed	Large Printed
L	mm	0.080	9.43	31.8
Scale	---	**1**	**118**	**398**
E_{poly}	GPa	1.0	0.60	0.60
E_{piezo}	GPa	56	56	80
t_{poly}	µm	5.0	593	2670
t_{piezo}	µm	1.2	120	480

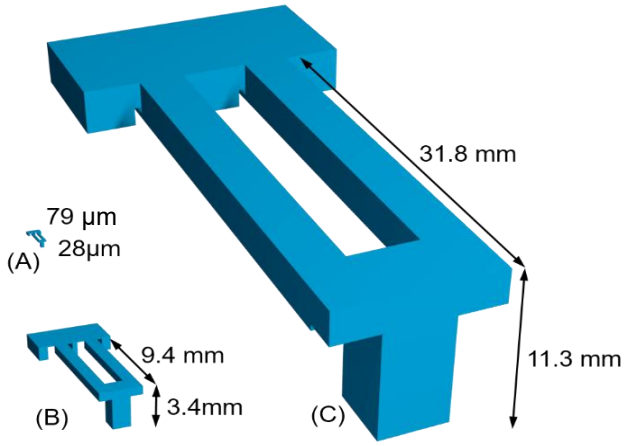

Figure 4. Size comparison of the three limbs. The Micro limb (A) uses a 1µm layer of thin film PZT with parylene polymer for the body. The Small Printed limb (B) uses a single layer PZT actuator with PLA polymer. the Large Printed limb (C) uses a double-layer PZT actuator and PLA polymer.

Analytical model for static behavior: In order to understand the basic static behavior of each limb, a simple analytical model was generated using linear beam-bending analysis. A free body diagram of the limb is shown in Fig. 5 (Pg. 6). The two legs are treated as flexible, while the foot is assumed to be rigid. Next, the PZT and polymer legs are combined into a single flexible beam with combined young's modulus and an effective neutral bending axis (based on [12]). The primary inputs are the bending moments M_{act} from the PZT actuators (calculated using Eq. 9),

$$M_{act} = d_{31} V E_{piezo} w_p \bar{z} \qquad \text{(Eq. 9)}$$

where w_p is the width of the PZT strip in the y-direction, and $\bar{x}$ is the distance from the center of the PZT strip to the neutral bending axis. This analysis assumes a single-layer PZT actuator for all devices, including the Large Printed device where the actual actuator was double-layered.

An additional input includes the reaction force at the base of the foot (R, shown in Eq. 10),

$$R = \begin{bmatrix} R_x \\ R_y \\ R_z \end{bmatrix} \qquad \text{(Eq. 10)}$$

where subscripts x, y, and z correspond to the components in the x, y, and z directions.

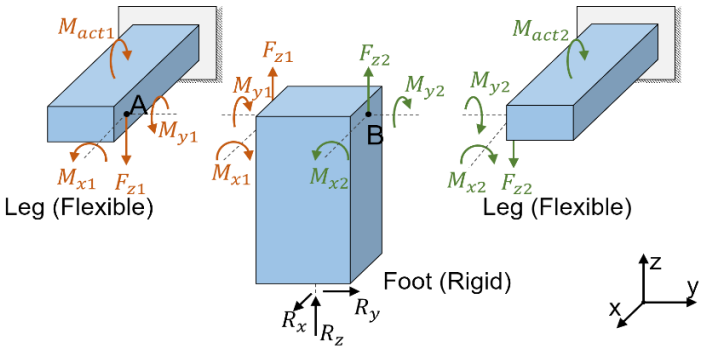

Figure 5. Free body diagram of the microrobotic limb. Sections were taken at points A and B. Inputs include bending moment from the PZT actuators and reaction forces at the foot. Outputs include vertical displacement of the foot and rotation of the foot about the x and y axes.

Outputs of interest include the vertical displacement of the foot (Δz) and rotation of the foot about the x and y axes (θ_x and θ_y) at each section point A and B. Outputs are included in the states X_1 and X_2, shown in Eq. 11-12.

$$X_1 = \begin{bmatrix} \Delta z_A \\ \theta_{xA} \\ \theta_{yA} \end{bmatrix}, \quad X_2 = \begin{bmatrix} \Delta z_B \\ \theta_{xB} \\ \theta_{yB} \end{bmatrix} \qquad \text{(Eq. 11-12)}$$

Next, all internal forces at the cuts (F_1, F_2) and the reaction forces (R) were related using force matrices (T_1, T_2), and a simple geometric factor (S) was used to relate the states at each side of the foot, as shown in Eq. 13 and 14.

$$T_1F_1 + T_2F_2 = T_RR, \qquad SX_1 = X_2 \qquad \text{(Eq. 13, 14)}$$

Then all flexible beams were considered using compliance matrices (C_1, C_2, C_{act1}, C_{act2}) to relate the input bending moments and internal forces to the states, as shown in Eq. 15 and 16,

$$X_1 = C_1F_1 + C_{act1}M_{act1}, \qquad X_2 = C_2F_2 + C_{act2}M_{act2} \qquad \text{(Eq. 15, 16)}$$

Solving this system of equations (Eq. 13-16) yields a model for the static behavior (X_1, X_2) as a function of voltage and contact forces, shown in Eq. 17

$$X_1 = [T_1C_1^{-1} + T_2C_2^{-1}S]^{-1}\,[T_RR + T_1C_1^{-1}C_{act1}M_{act1} + T_2C_2^{-1}C_{act2}M_{act2}] \qquad \text{(Eq. 17)}$$

M_{act1} and M_{act2} are calculated using Eq. 9, and X_2 is found using Eq. 14. Variables are described in greater detail in the appendix.

Finite element analysis for static behavior: In pursuit of a more accurate model for the static behavior of the static behavior of each-sized device, finite element analysis was performed (by Jinhong Qu) using COMSOL Multiphysics with the dimensions specified above. Models assumed linear material properties and a single-layer PZT actuator for all devices, including the Large Printed device where the actual actuator was double-layered.

Experimental characterization of dynamic behavior: The last step in this study was to fabricate a prototype device and test its behavior experimentally. The Large Printed limb was chosen to begin since it is easiest to fabricate and assemble. In order to avoid melting and large voids in the

printed parts, batches of six devices per print were used. After several batches, the device with the smallest number and size of voids was selected. To assemble the limb, first the PZT strips received two electrical leads each, bonded to the top and bottom surfaces using high-conductivity silver epoxy. After 3D printing the body, the PZT strips were attached to the plastic surface using general-purpose epoxy. The dimensions of the printed body were not fully confirmed, but are estimated to be within 10% of their specified values.

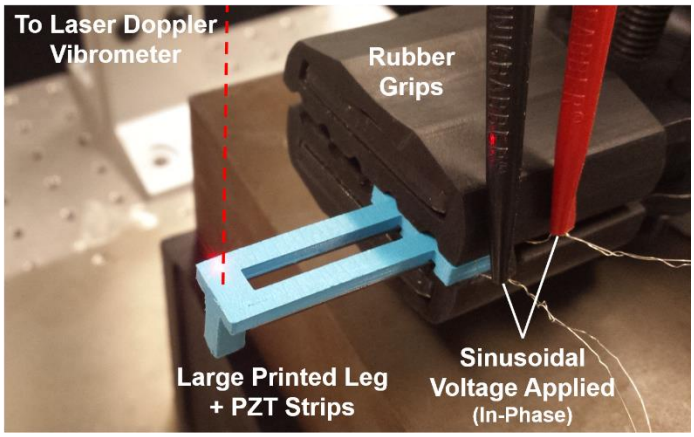

Figure 6. Testing setup for measuring the dynamic behavior of the fabricated limb device. Sinusoidal input voltages were applied in-phase during a frequency sweep from 10 to 10000 Hz, and the velocity of the foot was measured using a laser Doppler vibrometer.

Next, the dynamic behavior of the fabricated Large Printed limb was characterized, as shown in Fig. 6. The dynamic response was anticipated to be more easily and accurately measured for small displacements of the limb given available equipment. The device was held tightly in rubber grips, and a sinusoidal input voltage (amplitude of 18 V) was applied in-phase to the PZT actuators. Using a laser Doppler vibrometer, the velocity of the foot was measured and recorded using LabVIEW. A frequency sweep from 10 to 10000 Hz was performed, and a Bode plot was generated within LabVIEW. Approximately 7 averages were taken of smaller segments within the frequency sweep to obtain the full spectrum. The static behavior can then be inferred for comparison with model predications.

Results and Discussion

The results of modeling and experiments are compared and analyzed. FEA modeling for all three sizes of limbs is compared to determine how well the scaling analysis holds over different lengths and materials. Next, using the dynamic behavior of the fabricated Large Printed limb, the static behavior is extracted by examining the response and fitting the corresponding transfer function. Finally, analytical and FEA modeling is compared directly to the experimental results.

Comparison of scaling based on FEA: A comparison of the static responses (deflections vs. voltage and contact forces) of the three sizes of limbs, as predicted by FEA, is shown in Table 2.

Table 2: Static behavior, as predicted by FEA, does not exhibit scaling consistent with scaling analysis across all three limb sizes. The response relationships are non-dimensionalized and normalized to the Micro values.

Response Relationship	Pi Terms	Micro	Small Printed	Large Printed
Δz vs. Voltage (In-Phase)	Π_1 / Π_4	1	2.7	9.0
Δz vs. Voltage (Out of Phase)	Π_1 / Π_4	1	2.0	22.3
Δy vs. R_y	Π_2 / Π_5	1	1.8	36.0
Δz vs. R_z	Π_1 / Π_6	1	1.9	4.8

One would expect that if the earlier scaling analysis was holding all relevant groups constant, all three length scales would exhibit the same non-dimensional response. However, this is not the case in these results. Going from the Micro to Small-Printed limbs, there is a roughly uniform increase of around twice the value for all response relationships, indicating a possible trend captured due to neglecting pi terms in the scaling. However, there is no such trend going to the Large Printed limb, which does not appear to have increased linearly in any of the responses. Additionally, the discrepancy in responses were 2-4 times larger for the out-of-phase voltage and the y-direction reaction force. This could be due to the fact that the current scaling analysis does not take shear stress effects, such as shear modulus, fully into account. These effects would be anticipated to have greater effect as beam thickness to length ratio increases.

Dynamic and static behavior of the fabricated device: The response of the Large Printed limb's foot velocity (u_{tip}, in m/s) vs. input voltage (V_{in}, in Volts) as a function of frequency is shown in a bode plot in Fig. 7a (Pg. 8). The first resonance frequency is 350±1 Hz, and the damping ratio is 0.032±0.001, showing that the system is very underdamped, which is what we would expect for the device. We can approximate the first resonance mode as a simple cantilever beam. Since the response is measured using velocity vs. voltage applied, we obtain a transfer function describing the first resonance peak, as shown in Eq. 18.

$$\frac{u_{tip}}{V_{in}} = \frac{(K\omega_n^2)\, s}{s^2+2\zeta\omega_n+\omega_n^2} \qquad \text{(Eq. 18)}$$

where K is the DC gain, ω_n is natural frequency, ζ is damping ratio, and s represents a complex exponential. Next, this transfer function was fit to the data near the first resonance peak, allowing for the characterization of the parameters including the DC gain, which represents the foot deflection (Δz) at a constant voltage. This yielded a static displacement vs. actuator voltage slope of 0.035±0.001 μm/V, which is relatively small.

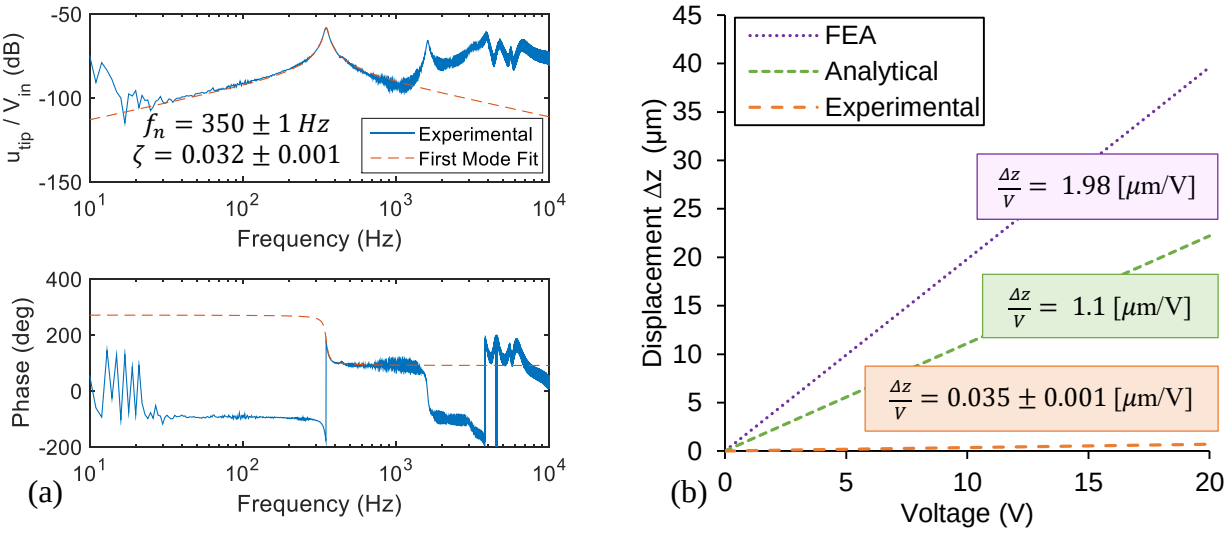

Figure 7. Dynamic behavior of fabricated Large Printed limb yields static behavior, which is less than expected compared to model predictions. The bode plot (a) show the frequency response of the fabricated device with first-mode fit overlayed. Based on this fit, the static deflection of the foot as a function of voltage is found and compared to that predicted by the models (b). The two modeling techniques produce similar order of magnitude results, however the fabricated device is two orders of magnitude smaller.

Comparison of experimental behavior to model predictions: A comparison of experimental static behavior of the Large Printed limb to behavior predicted by the analytical and FEA models is shown in Fig. 7b (Pg. 8). The displacement vs. voltage response of the two modeling techniques are in fairly good agreement with each other (in and order-of-magnitude sense). The analytical model predicts a smaller deflection than the FEA for a unit voltage. The experimental response, however, is two orders of magnitude smaller than predicted by the models. This discrepancy could be due to energy loss in the epoxy layer during oscillation, or perhaps due to the PZT strip having a double-layer structure with oppositely polarized layers. If the neutral bending axis is too far from the center of the PZT strip, one of the layers could be expanding or contacting in the opposite direction than is necessary to bend the beam, making the actuator less effective than expected. In addition, the elastic modulus of the PLA body after printing is incompletely characterized, and would benefit from dedicated testing.

Conclusions

From the experiments, modeling, and analysis performed in this study, we conclude that 3D printing shows promise for prototyping thin-film PZT/polymer microrobots. Specifically, we found that integrating PZT into the printing process is non-trivial, but even without such capability a variety of integrated structures may be feasible. Additionally, we created analytical and FEA models for a simple microrobotic limb design that predict static behavior relatively close to each other. The fabricated Large Printed limb exhibited resonance behavior, as expected, however the static behavior is much smaller than the models predict. This may be caused by the fabricated device exhibiting a different structure than what was modeled. Finally, the scaling analysis produces predictable results for the small printed device, but fails for the large printed device. This could be caused by neglecting to keep some pi terms constant, and possibly due to poor account of shear in the analysis. Understanding how prototype behavior corresponds to micro-scale can help bridge the gap for the microrobot design process as well the study of micro-contact dynamics. Further, if meso-scale 3D printed robots can exhibit behavior similar to micro-scale robots, there is potential to move to using the 3D printed robots for similar applications since they are much cheaper and easier to make.

Future Work

Based on our analysis of experiments and modeling, there are several pieces of work to be done to obtain more accurate values and better agreement between models and experiments. First, it is imperative that we revisit the scaling analysis to determine if there are better ways to account for the terms that were not held constant, and perhaps look into how to best account for shear stress effects. In addition, performing a similar analysis of scaling behavior using the analytical model could yield some understanding of what terms are most important. Next, fabrication of the Small Printed limb would give us a better understanding of how models and experimental results compare. Its fabricated structure will be more similar to the FEA and analytical models than the Large Printed limb, and its dimensions will also more closely approach the eventual Micro-Scale limb dimensions. From there, finding ways to integrate piezoelectric strips into the 3D printing process could help improve any epoxy energy-loss problems. Final designs used during characterization of the 3D printing process will then be incorporated into future wafer-level microrobot fabrication batches. This will provide a direct test of the scaling analysis. Lastly, testing this prototyping process on more complicated microrobot geometries will provide insight into the robustness of the process.

References

[1] B. Watson, J. Friend and L. Yeo, "Micromotor of Less Than 1 mm^3 Volume for In Vivo Medical Procedures," *Third International Conference on Quantum, Nano and Micro Technologies,* 2009.

[2] P. Chirarattananon, K. Y. Ma and R. J. Wood, "Adaptive Control for Takeoff, Hovering, and Landing of a Robotic Fly," *International Conference on Intelligent Robots and Systems,* 2013.

[3] M. Takato, S. Yamasaki, S. Takahama, J. Tanida, K. Saito and a. F. Uchikoba, "Insect Type MEMS Micro Robot Controlled by CMOS IC of Hardware Neural," *ECAL,* 2013.

[4] M. Shin, J. Choi, R. Q. Rudy, C. Kao, J. S. Pulskamp, R. G. Polcawich and K. R. Oldham, "(Presenation) Micro-Robotic Actuation Units Based on Thin-Film Piezoelectric and High-Aspect Ratio Polymer Structures," in *IDETC/CIE*, Buffalo, NY, 2014.

[5] M. Shin, J. Choi, R. Q. Rundy, C. Kao, J. S. Pulskamp, R. G. Polcawich and K. R. Oldham, "Micro-robotic actuation units based on thin-film piezoelectric and highsaspect ratio polymer structures," in *IDETC/CIE 2014*, Buffalo, New York, 2014.

[6] C.-H. Rhee, "Design and Fabrication of Robust High Performance Piezoelectric Micro-Devices," *Doctoral Dissertation,* 2012.

[7] J. H. Ryou, "Foot Impact and Dynamic Analyses of Piezoelectrically-Actuated Walking Micro-Robots," *Doctoral Dissertation,* 2013.

[8] G. V. Kaigala, S. Ho, R. Penterman and C. J. Backhouse, "Rapid prototyping of microfluidic devices with a wax printer," *Lab on a Chip,* 2007.

[9] A. Bertsch, P. Bernhard, C. Vogt and P. Renaud, "Rapid prototyping of Small Size Objects," *Rapid Prototyping Journal,* 2000.

[10] A. M. Hoover and R. S. Fearing, "Fast scale prototyping for folded millirobots," *IROS,* 2008.

[11] Ultimaker B.V., "Ultimaker Original - Support," Ultimaker B.V., 2015. [Online]. Available: https://ultimaker.com/en/support/ultimaker-3d-printers/ultimaker-original.

[12] I. A. Assakkaf, "Beams: Composite Beams; Stress Concentrations," Dept. Civil and Environmental Engineering, University of Mayland, College Park, 2003.

Appendix

Analytical model for static behavior: Continuing from Pg. 6, the compliance matrices (*C*) were found using standard cantilever beam deflections, as shown in Eq. 19, 20,

$$C_1 = \begin{bmatrix} -\frac{L^3}{2EI} & 0 & -\frac{L^2}{2EI} \\ -\frac{L}{2cH^3G} & -\frac{L}{cWH^3G} & 0 \\ -\frac{L^2}{EI} & 0 & -\frac{L}{EI} \end{bmatrix}, \quad C_2 = \begin{bmatrix} \frac{L^3}{2EI} & 0 & \frac{L^2}{2EI} \\ -\frac{L}{2cH^3G} & \frac{L}{cWH^3G} & 0 \\ \frac{L^2}{EI} & 0 & \frac{L}{EI} \end{bmatrix} \quad \text{(Eq. 19, 20)}$$

where *L*, *H* and *W* are the length (x-dir), thickness (z-dir) and width (y-dir) of the leg, *E* is the combined elastic modulus, G is shear modulus of the polymer, *c* is the torsional factor (assumed to be 0.333), *I* is the second moment of area of the rectangular leg ($H^3W/12$).

Next, the internal reactions forces at each cut were related using force matrices (*T*), as shown in Eq. 21-23.

$$T_1 = \begin{bmatrix} 1 & 0 & 0 \\ 0 & 0 & -1 \\ -w/2 & 1 & 0 \end{bmatrix}, \quad T_2 = \begin{bmatrix} -1 & 0 & 0 \\ 0 & 0 & 1 \\ -w/2 & -1 & 0 \end{bmatrix}, \quad T_R = \begin{bmatrix} 0 & 0 & -1 \\ -h & 0 & 0 \\ 0 & -h & 0 \end{bmatrix} \quad \text{(Eq. 21-23)}$$

where *w* and *h* are the width (y-dir) and thickness (z-dir) of the foot.

The geometric relationship (*S*) between X_1 and X_2 was found using trigonometric relations, and linearized using small-angle approximations. The result is shown in Eq. 24.

$$S = \begin{bmatrix} 1 & -w & 0 \\ 0 & 1 & 0 \\ 0 & 0 & -1 \end{bmatrix} \quad \text{(Eq. 24)}$$

Finally, using Eq. 13-16, the static response of the limb (X_1) was found as a function of voltage, shown in Eq. 17, where M_{act1} and M_{act2} are calculated using Eq. 9, and X_2 is found using Eq. 14.